Disruption of ceruloplasmin and hephaestin in mice causes retinal iron overload and retinal degeneration with features of age-related macular degeneration

Paul Hahn*, Ying Qian*, Tzvete Dentchev*, Lin Chen*, John Beard†, Zena Leah Harris‡, and Joshua L. Dunaief*§

*The F. M. Kirby Center for Molecular Ophthalmology, Scheie Eye Institute, University of Pennsylvania, Philadelphia, PA 19104; †Department of Nutrition, College of Health and Human Development, Pennsylvania State University, University Park, PA 16802; and ‡Department of Anesthesiology and Critical Care Medicine, Division of Pediatric Anesthesiology and Critical Care Medicine, The Johns Hopkins University, Baltimore, MD 21287

Communicated by Stirling A. Colgate, Los Alamos National Laboratory, Los Alamos, NM, July 30, 2004 (received for review January 10, 2004)

Mechanisms of brain and retinal iron homeostasis have become subjects of increased interest after the discovery of elevated iron levels in brains of patients with Alzheimer's disease and retinas of patients with age-related macular degeneration. To determine whether the ferroxidase ceruloplasmin (Cp) and its homolog hephaestin (Heph) are important for retinal iron homeostasis, we studied retinas from mice deficient in *Cp* and/or *Heph*. In normal mice, Cp and Heph localize to Müller glia and retinal pigment epithelium, a blood–brain barrier. Mice deficient in both *Cp* and *Heph*, but not each individually, had a striking, age-dependent increase in retinal pigment epithelium and retinal iron. The iron storage protein ferritin was also increased in *Cp*−/−*Heph*−/*Y* retinas. After retinal iron levels had increased, *Cp*−/−*Heph*−/*Y* mice had age-dependent retinal pigment epithelium hypertrophy, hyperplasia and death, photoreceptor degeneration, and subretinal neovascularization, providing a model of some features of the human retinal diseases aceruloplasminemia and age-related macular degeneration. This pathology indicates that Cp and Heph are critical for CNS iron homeostasis and that loss of Cp and Heph in the mouse leads to age-dependent retinal neurodegeneration, providing a model that can be used to test the therapeutic efficacy of iron chelators and antiangiogenic agents.

Iron is an essential cofactor in heme and nonheme-containing enzymes, but ferrous iron (Fe^{2+}) generates free radicals that can cause oxidative damage via the Fenton reaction. Homeostatic regulation of ferrous iron levels is critical for meeting physiologic demand while preventing the toxicity associated with iron overload.

Consistent with a need for precise regulation of retinal iron, iron overload can cause retinal degenerations. Iron retained in the eye as a foreign body or injected into the vitreous causes photoreceptor degeneration, demonstrating that iron overload is toxic to photoreceptors (1–3). A comparison of postmortem retinas from age-related macular degeneration (AMD) and normal donors documented increased iron within the retinal pigment epithelium (RPE) (4), a cellular monolayer forming the blood-retinal barrier and nourishing photoreceptors. These results suggest that iron overload may play a role in the pathogenesis of AMD, a retinal degeneration that is the most common cause of irreversible vision loss in the U.S.

Iron overload is also implicated in the retinal degeneration occurring in patients with the rare autosomal recessive disease aceruloplasminemia. These patients have pathologic accumulation of iron in liver, spleen, pancreas, retina, and basal ganglia by the fourth or fifth decade of life (5, 6). Five Japanese patients all had pigmentary retinopathy by their fifth decade (5–7). Although histopathology has not been published, one patient had retinal iron overload in unspecified cell types (6). One Caucasian patient with undetectable serum ceruloplasmin had drusen, yellowish white spots under the retina that constitute the defining clinical feature of AMD (J.L.D., unpublished results). Because this patient's drusen were first detected at age 46, an early onset of AMD, this finding further suggests a link between retinal iron overload and AMD.

Ceruloplasmin (Cp) is a multicopper ferroxidase produced by alternate splicing as either a membrane-linked (8) or secreted protein. The secreted form circulates in the blood but does not cross the blood–brain barrier (8). Thus, to function beyond the blood–retinal barrier, *Cp* must be expressed in the retina. Within the normal human and mouse retinas, *Cp* expression was detected in the inner nuclear layer (9, 10), with increased expression in the inner nuclear layer and ganglion cell layer after optic nerve crush (11) and an increase in Müller glia after photic injury (12).

Evidence suggests that Cp facilitates iron export from cells. By oxidizing ferrous to ferric iron, the only form that can be taken up by the serum transport protein, transferrin, Cp may establish an ion gradient favoring iron export. *In vitro*, Cp is necessary for iron export from brain astrocytes (13) and can facilitate iron export from macrophages (14). Further, *Cp*−/− mice have impaired liver iron efflux (15). Unlike humans with aceruloplasminemia, our *Cp*−/− mice do not manifest significant CNS iron overload or neuropathy even at 24 months. An independently generated *Cp*−/− mouse showed mild CNS iron overload, and cells from these mice had increased susceptibility to oxidative stress (16).

One potential explanation for the lack of severe CNS iron overload in *Cp*−/− mice is that hephaestin (Heph), another multicopper ferroxidase with 50% identity to Cp, may also facilitate iron export. *Heph* is naturally mutated in the *sex-linked anemia* (*sla*) mouse (17). Because Heph is a membrane-bound protein that mediates iron egress from intestinal enterocytes into the circulation (17), *sla* mice are anemic as a result of impaired intestinal iron absorption. The *Heph* mutation in the *sla* mouse is a deletion of two exons resulting in a predicted deletion of 194 aa. As a result, *sla* mice have significantly diminished Heph ferroxidase activity (18).

Before the present study, Heph had not to our knowledge been studied in the retina. To test the hypothesis that deficiency of both Cp and Heph would induce retinal iron overload and neurodegeneration, we generated mice harboring both our Cp knockout allele and the sex-linked *Heph* mutation from *sla* mice and studied male mice herein referred to as *Cp*−/−*Heph*−/*Y* mice. We find that combined deficiency of Cp and Heph results in retinal iron accumulation with secondary increases in several forms of the iron storage protein ferritin and, ultimately, retinal degeneration.

Methods

Generation of Mice and Fixation of Eyes. C57BL/6 mice with a targeted mutation in the Cp gene (*Cp*−/−) (15), C57BL/6 mice with the naturally occurring *sla* mutation in the Heph gene (designated herein as *Heph*−/*Y*, as *Heph* resides on the X chromo-

Abbreviations: Cp, ceruloplasmin; Heph, hephaestin; AMD, age-related macular degeneration; RPE, retinal pigment epithelium; CRALBP, cellular retinaldehyde binding protein; DAB, 3,3′-diaminobenzidine.

§To whom correspondence should be addressed. E-mail: jdunaief@mail.med.upenn.edu.

www.pnas.org/cgi/doi/10.1073/pnas.0405146101

some), and mice generated by crossing both single knockout mice (*Cp*−/−*Heph*−/*Y*) were studied. Eyes were enucleated immediately after death and fixed overnight in 4% paraformaldehyde with or without 0.5% glutaraldehyde or in 10% formalin. In addition, WT C57BL/6 and BALB/c eyes were enucleated and lightly fixed in 4% paraformaldehyde for 2 h before use for immunohistochemistry. All procedures were approved by the Institutional Animal Care and Use Committee of the University of Pennsylvania. Human eyes were obtained from the National Disease Research Interchange through a protocol approved by the University of Pennsylvania Institutional Review Board. They were enucleated 3 h postmortem and kept on ice until retinas were dissected 24 h later and used for Western analysis.

Dissection of Murine RPE and Retinas for RT-PCR and Western Analysis. C57BL/6 mice were killed, and eyes were promptly enucleated. Anterior segments were removed, and retinas were completely dissected away from the underlying RPE. Retinas were then flash-frozen and stored at −80°C. RPE was enzymatically detached from the remaining posterior segment by incubation in 0.25% trypsin at 37°C, 5% CO_2 for 20 min. Detached RPE was collected in an Eppendorf tube, pelleted, flash-frozen, and stored at −80°C.

RT-PCR. RNA was extracted from primary murine RPE and spontaneously immortalized human ARPE-19 cells (19) by using TRIzol (GIBCO/BRL) and used to generate first-strand cDNA with a T7-(dT)24-mer primer and the SuperScript II reverse transcriptase (GIBCO). Specific sequences were then amplified by PCR using a PTC-0200 thermocycler (MJ Research, Cambridge, MA).

Primers for rod opsin, RPE65, Cp (amplifying both the secreted and glycosylphosphatidylinositol-linked forms), and Heph were designed to span intron–exon boundaries within genomic DNA to amplify cDNA and minimize amplification of potentially contaminating genomic DNA. The murine opsin forward primer was 5′-TCTTCACAGTCAAGGAGGCG-3′, with a reverse primer of 5′-ACAGCGTGGTGAGCATACAG-3′. For murine RPE65, the designed forward primer was 5′-TTACGTGAGAATTGGGAAGAAG-3′, and the reverse primer was 5′-AGGATCTTTTGAACAGTCCATG-3′. The murine Cp forward primer was 5′-ACAGTTGTTCCAACGTTACC-3′, whereas the reverse primer was 5′-ACTCCCCTGTGCTTGTATTG-3′. The human Cp forward primer was 5′-CCACAAGGCCCTACTCAATAC-3′, and the reverse primer was 5′-AACAGAAGGGCAAATTCCAG-3′. For murine Heph, the forward primer was 5′-CAAAGTTACAGGGCAGATGTGGTG-3′, and the reverse primer was 5′-CCAGAGCAATGAGCAACAGAAGC-3′. The human Heph forward primer was 5′-TGGGAAACTCTATGCCAACCTTAG-3′, and the reverse primer was 5′-ATGGACCTCCTATTGCGTCGTAGC-3′.

Western Analysis. Protein from normal human retinas, murine retinas, and cultured cell lines (ARPE-19 and rMC-1) was isolated and subjected to Western analysis as described in ref. 12 by using rabbit anti-Cp (DAKO; 1:1,000) or rabbit anti-Heph (Alpha Diagnostic, San Antonio, TX; 1:1,000) antibodies.

Histochemical Iron Detection. Paraffin sections (5 μm thick) prepared from whole globes were Perls' stained by incubation in 5% potassium ferrocyanide in 5% aqueous hydrochloric acid for 30 min at room temperature, yielding a Prussian blue reaction product. Sensitivity for iron detection was enhanced by subsequent incubation in 0.75 mg/ml 3,3′-diaminobenzidine (DAB) and 0.00075% H_2O_2 for 30 min at room temperature, yielding a brown reaction product. As the Perls' reaction product was found in pigmented RPE, sections were bleached by incubation overnight in 3% H_2O_2 before staining to improve visibility of Perls' signal. Sections were analyzed by light and fluorescence microscopy with a Nikon TE-300 microscope and a SpotRT Slider camera (Diagnostic Instruments, Sterling Heights, MI) with IMAGEPRO PLUS software, Version 4.1 (Media Cybernetics, Silver Spring, MD).

Quantitative Iron Detection. Retinas from WT, *Cp*−/−, *Heph*−/*Y*, and *Cp*−/−*Heph*−/*Y* mice were dissected from the underlying RPE/choroid/sclera. Iron in these tissues was measured by graphite furnace atomic absorption spectrophotometry (model 5100 AA, PerkinElmer) by using standard methods (20).

Electron Microscopy and Energy-Dispersive X-Ray Spectroscopy. Retinas (including RPE) fixed in 2% paraformaldeyhyde, 2% glutaraldehyde were postfixed in 1% osmium tetroxide, 0.1 M sodium cacodylate buffer. Specimens were dehydrated and embedded in Epon (Ted Pella, Inc., Redding, CA). Ultrathin sections were cut, stained with uranyl acetate, and examined with a JEOL 1010 transmission electron microscope. Semithin 1- to 3-μm sections were stained with toluidine blue or methylene blue/azure II and analyzed by light microscopy as described above.

Energy-dispersive x-ray spectroscopy was performed with scanning mode, and spectra were collected with a Kevex 8000 energy-dispersive x-ray spectrometer (Thermo Electron, Peabody, MA) installed on an H-600 electron microscope (Hitachi, Pleasanton, CA), as described in ref. 21 on 200-nm-thick sections without any secondary stain.

Immunohistochemistry. Fixed globes were rinsed in PBS and prepared as eyecups, which were treated with 0.1% sodium borohydride (if fixed in glutaraldehyde), cryoprotected in 30% sucrose, and embedded in Tissue-Tek OCT (Sakura Finetek, Torrance, CA).

Immunohistochemistry was performed on cryosections 10 μm thick as published in ref. 22. Primary antibodies were rabbit anti-Heph (1:500; J. Gitlin, Washington University, St. Louis), mouse anti-cellular retinaldehyde binding protein (CRALBP) (1:250; J. Saari, University of Washington, Seattle), rabbit anti-light ferritin (F17), and heavy ferritin (Y17) [both 1:2,500; P. Santambrogio (Instituto di Ricovero e Cura a Carattere Scientifico, Milan) and P. Arosio (University of Brescia, Brescia, Italy)]. Control sections were treated identically but with omission of primary antibody. Specificity of ferritin immunoreactivity was confirmed by preincubation of antibody with a 5 M excess of antigenic or unrelated protein. Sections were analyzed by fluorescence microscopy using identical exposure parameters across genotypes as described above.

Results

***Cp* and *Heph* Are Expressed in RPE.** To investigate normal expression of *Cp* and *Heph*, RT-PCR analysis was performed on RPE dissected from C57BL/6 mice. In two different experiments, one from a single 6-month-old C57BL/6 mouse (Fig. 1*A*) and another from three mice 3, 5, and 7 months old, respectively (data not shown), both *Cp* and *Heph* mRNAs were detected in RPE. To confirm RPE expression of *Cp* and *Heph*, RT-PCR analysis was also performed on the human ARPE-19 cell line (19). As with the dissected mouse RPE, ARPE cells expressed *Cp* and *Heph*. The purity of isolated RPE was demonstrated by amplification of RPE65, an RPE-specific gene, but not opsin, a retina-specific gene.

Cp and Heph Proteins Are Present in Müller Glia and RPE. Consistent with the RT-PCR results, Western analysis detected both Cp and Heph proteins in ARPE-19 cells. Both proteins were also present in mouse and human retina and rMC-1 cells, a rat Müller glial cell line, with Cp protein migrating at ≈130 kDa and Heph at ≈150 kDa (Fig. 1*B*). Cp from human tissue (purified plasma Cp and ARPE-19) migrated slightly slower than from rodent tissue (mouse retina and rMC-1).

We and others demonstrated by immunohistochemistry that Cp protein is present diffusely throughout the murine retina,

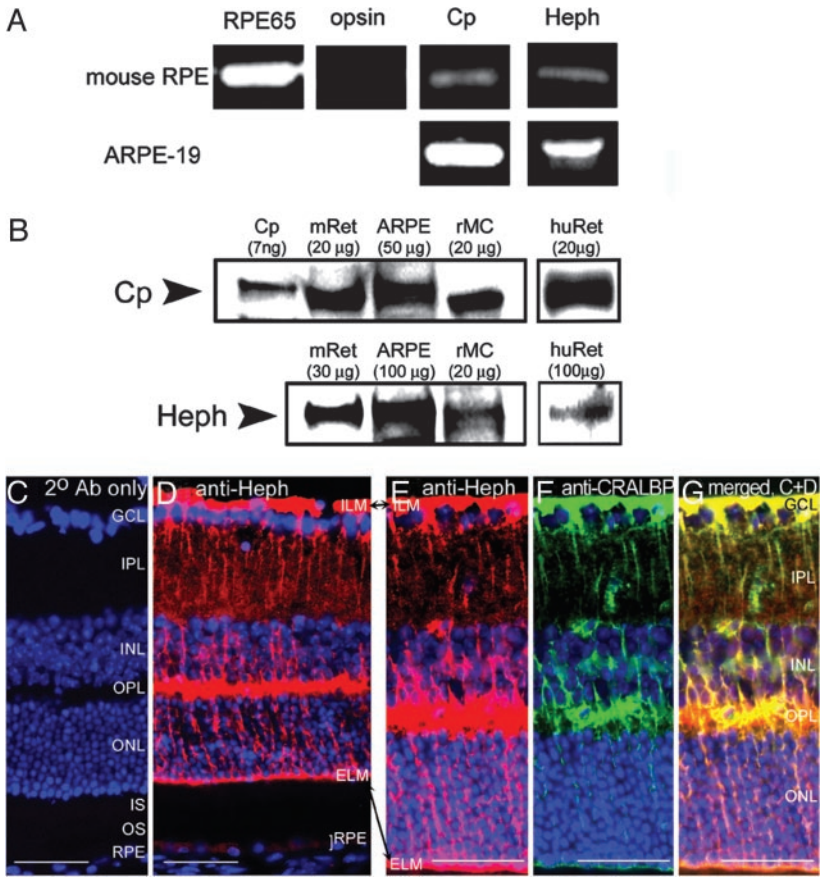

Fig. 1. Cp and Heph mRNA and proteins are present in normal RPE and retina within Müller cells. (*A*) Bands from ethidium bromide-stained agarose gels corresponding to RT-PCR amplification products of the indicated mRNAs from dissected C57BL/6 murine RPE and cultured ARPE-19 cells. In all cases, the amplification product was of the expected size. (*B*) Western analysis of Cp and Heph in dissected C57BL/6 murine retinas (mRet) human retinas (huRet), cultured ARPE-19 cells, and cultured rMC-1 cells. Purified human Cp (labeled Cp) was used as control. (*C*) Control BALB/c retina labeled with a Cy3-conjugated donkey anti-rabbit secondary antibody. (*D*) Normal BALB/c retina immunolabeled for Heph. (*E–G*) Normal BALB/c retina double-labeled with anti-Heph and anti-CRALBP, a marker for Muller glia. A single red exposure reveals anti-Heph immunoreactivity (*E*). A single green exposure shows anti-CRALBP immunoreactivity (*F*). Double exposure shows yellow colocalization of Heph and CRALBP (*G*). (Scale bars: 50 μm.)

particularly in Müller cells whose Cp levels increase after retinal stress (11, 12). Similarly, Heph localizes to Müller cells as identified by colabeling with anti-Heph and CRALBP, a Müller cell and RPE marker (Fig. 1*G*). Heph was present in Müller cell bodies within the inner nuclear layer and in Müller cell processes extending radially through the retina. Highest levels of Heph were found in the Müller endfeet adjacent to the internal limiting membrane at the inner surface of the retina.

Weak Heph immunofluorescence was present in RPE cells. This modest RPE immunofluorescence was greater than that of the 2º antibody-only control (Fig. 1*C*). Even though the control was intentionally imaged with a $\times 10$ longer exposure time than the other panels in Fig. 1, no signal was present. The faint Heph signal in the RPE (Fig. 1*D*) is consistent with the RT-PCR (Fig. 1*A*) and Western data (Fig. 1*B*), indicating that Heph mRNA and protein are present in the RPE.

At age 5–6 months, *Cp*−/−*Heph*−/*Y* retinas have increased iron, with highest levels in the RPE and photoreceptor outer segments. Because *Cp* and *Heph* mRNAs and proteins are present in retina and RPE, retinas deficient in these ferroxidases ($n = 5$ for each genotype) were analyzed by the Perls' stain for iron to determine whether their deficiency would result in iron accumulation. Iron in all normal, *Cp*−/−, and *Heph*−/*Y* retinas studied (up to 9 months old) was below the limits of detection by Perls' stain (Fig. 2 *A* and *B*) even with DAB enhancement (Fig. 2*F*). In contrast, all *Cp*−/−*Heph*−/*Y* retinas >5 months old ($n = 5$) had a striking granular Perls' stain in the RPE (Fig. 2 *C* and *D*); DAB enhancement further detected regional photoreceptor outer segment iron in *Cp*−/−*Heph*−/*Y* retinas (Fig. 2*E*).

At the ultrastructural level, the RPE of 5- to 6-month-old *Cp*−/−*Heph*−/*Y* but not WT or single knockout eyes contained electron-dense vesicles visible without Perls' staining. These single-membrane enclosed vesicles were most likely lysosomes or endosomes, sometimes fused with melanosomes (Fig. 2*G*). Energy-dispersive x-ray spectroscopy showed that the electron-dense particles had high iron peaks, at least four times higher than in melanosomes or other cytoplasmic locations in the WT RPE or outside of the vesicles in the *Cp*−/−*Heph*−/*Y* RPE.

To quantify iron accumulation, dissected sclera/choroid/RPE and dissected neural retinas (without RPE) from 7-month-old mice were analyzed by atomic absorption spectrophotometry. There was little difference between WT, *Cp*−/−, and *Heph*−/*Y* tissues, whereas the *Cp*−/−*Heph*−/*Y* tissue had significant increases in iron. When *Cp*−/−*Heph*−/*Y* tissues ($n = 3$) were compared to non-*Cp*−/−*Heph*−/*Y* tissues ($n = 4$), sclera/choroid/RPE had a 4.2-fold increase in *Cp*−/−*Heph*−/*Y* compared to non-*Cp*−/−*Heph*−/*Y* tissue (mean ± SEM, expressed in μg of iron per g of tissue: 194.2 ± 34.3 vs. 48.3 ± 11.1, $P < 0.04$). *Cp*−/−*Heph*−/*Y* retinas had a 3.6-fold increase in iron compared to non-*Cp*−/−*Heph*−/*Y* retinas (19.1 ± 3.4 vs. 5.2 ± 1.2, $P < 0.04$). This RPE and photoreceptor iron accumulation appears to be age-dependent, as no iron was detectable in a 4-week-old *Cp*−/−*Heph*−/*Y* retina by DAB-enhanced Perls' stain (data not shown).

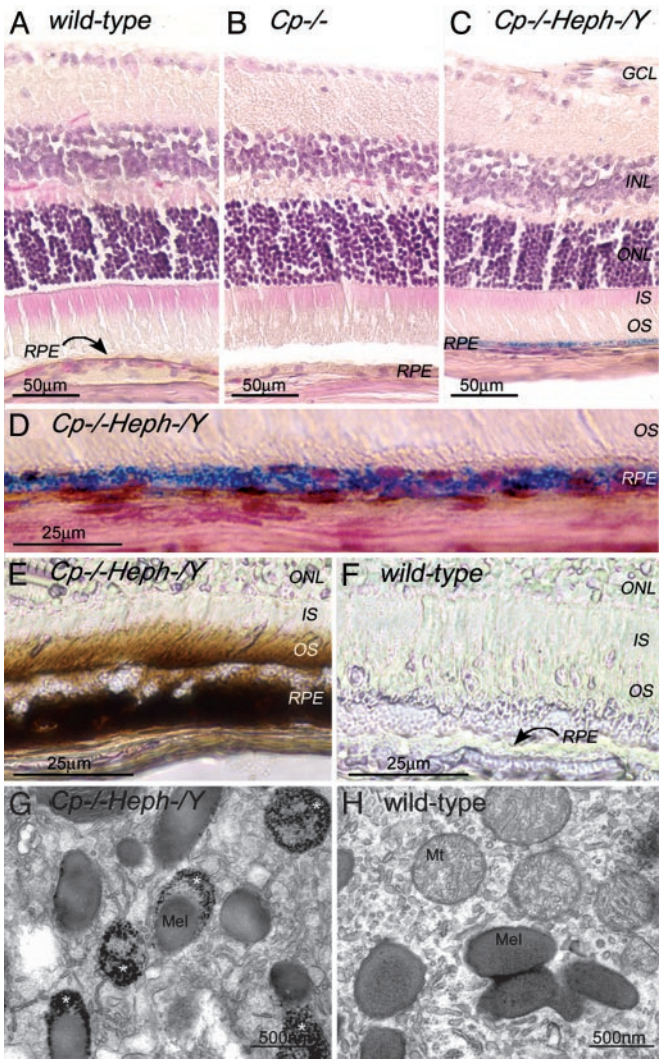

Fig. 2. Adult (6-month-old) *Cp−/−Heph−/Y* RPE and photoreceptors accumulate iron. (*A–C*) 6-month-old WT (*A*), *Cp−/−* (*B*), and *Cp−/−Heph−/Y* (*C*) retinas Perls' stained for iron (blue) and counterstained with hematoxylin/eosin. (*D*) High magnification of Prussian blue Perls' label in 6-month-old *Cp−/−Heph−/Y* RPE. (*E* and *F*) Light photomicrographs of 6-month-old *Cp−/−Heph−/Y* (*E*) and WT (*F*) retinas after DAB enhancement (brown) of Perls' stain. (*G–H*) Electron micrographs of RPE from 6-month-old *Cp−/−Heph−/Y* (*G*) and WT (*H*) eyes. Only the *Cp−/−Heph−/Y* RPE (*G*) contains electron-dense vesicles (*) sometimes fused with melanosomes.

Levels of Ferritins Are Increased in *Cp−/−Heph−/Y* Retinas. Levels of the cytosolic iron storage protein ferritin are controlled by intracellular iron levels; through the iron regulatory proteins IRP1 and IRP2, increased iron leads to increased cytosolic ferritin mRNA translation, leading to increased ferritin protein levels (23). Ferritin multimers are composed of heavy (H) and light (L) chains. To determine whether increased iron in 5- to 6-month-old *Cp−/−Heph−/Y* retinas is accompanied by increased ferritin, retinas ($n = 4$ from each genotype) were immunolabeled with anti-H-ferritin and anti-L-ferritin (Fig. 3). H- and L-ferritin immunoreactivity was much stronger in the *Cp−/−Heph−/Y* retinas than in *Cp−/−*, *Heph−/Y* (data not shown), or WT, consistent with the increased retinal iron detected by atomic absorption spectrophotometry. Both H- and L-ferritin were present among all genotypes in bipolar cell synaptic terminals in the inner plexiform layer. Additionally, H-ferritin immunoreactivity (Fig. 3 *A–C*) across all genotypes

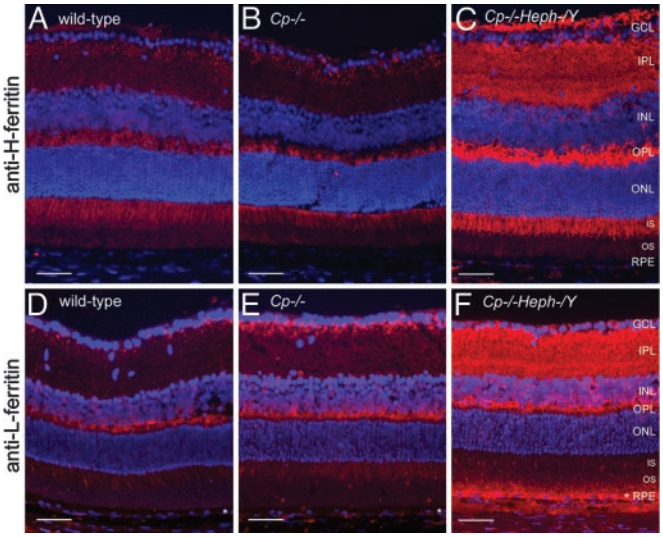

Fig. 3. *Cp−/−Heph−/Y* retinas have increased ferritin. Fluorescence photomicrographs of 6-month-old WT, *Cp−/−*, and *Cp−/−Heph−/Y* retinas immunolabeled for H-ferritin (*A–C*) and L-ferritin (*D–F*) and imaged by using identical exposure parameters. (Scale bars: 50 μm.)

was strongest in photoreceptors, including their inner segments and axons in the outer part of the outer plexiform layer, whereas L-ferritin (Fig. 3 *D–F*) was localized to the inner aspect of the outer plexiform layer, the bipolar synaptic terminals, and RPE.

***Cp−/−Heph−/Y* Mice Surviving to 6–9 Months Exhibit Retinal Degeneration.** Retinas from *Cp−/−Heph−/Y* mice surviving to age 6–9 months ($n = 3$) all had severe pathologic abnormalities. At the gross level, there were focal areas of hypopigmentation in the midperipheral retina, the largest spanning approximately one-third of the distance from optic nerve to the anterior edge of the retina (Fig. 4). Histology described below suggests that decreased concentration of RPE pigment caused by RPE hypertrophy and RPE death as well as underlying choroidal thinning account for the hypopigmentation.

The RPE cells in affected *Cp−/−Heph−/Y* but not age-matched WT retinas were massively hypertrophic in up to half the eye in confluent stretches spanning up to ≈75% of the length of the retina in a given section (Fig. 5*C*) and in the remainder of the eye in focal patches comprising a few hypertrophic cells (Fig. 5*B*). Electron microscopy analysis of these hypertrophic *Cp−/−Heph−/Y* RPE demonstrated numerous phagosomes and lysosomes containing partially digested photoreceptor outer segment membranes (Fig. 5*G*). Electron-dense vesicles were also observed in these affected 6- to 9-month-old *Cp−/−Heph−/Y* RPE, similar to those observed in the histologically normal, younger *Cp−/−Heph−/Y* RPE.

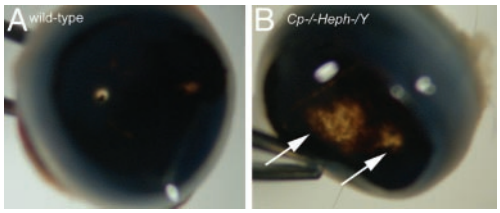

Fig. 4. Gross photomicrograph of atrophy in 9-month-old *Cp−/−Heph−/Y* retina. After removal of the cornea and lens, WT eye cup (*A*) has transillumination only at the optic nerve. In contrast, *Cp−/−Heph−/Y* eye cup (*B*) has areas of depigmentation (arrows) consistent with RPE pigment loss and atrophy in the peripheral retina.

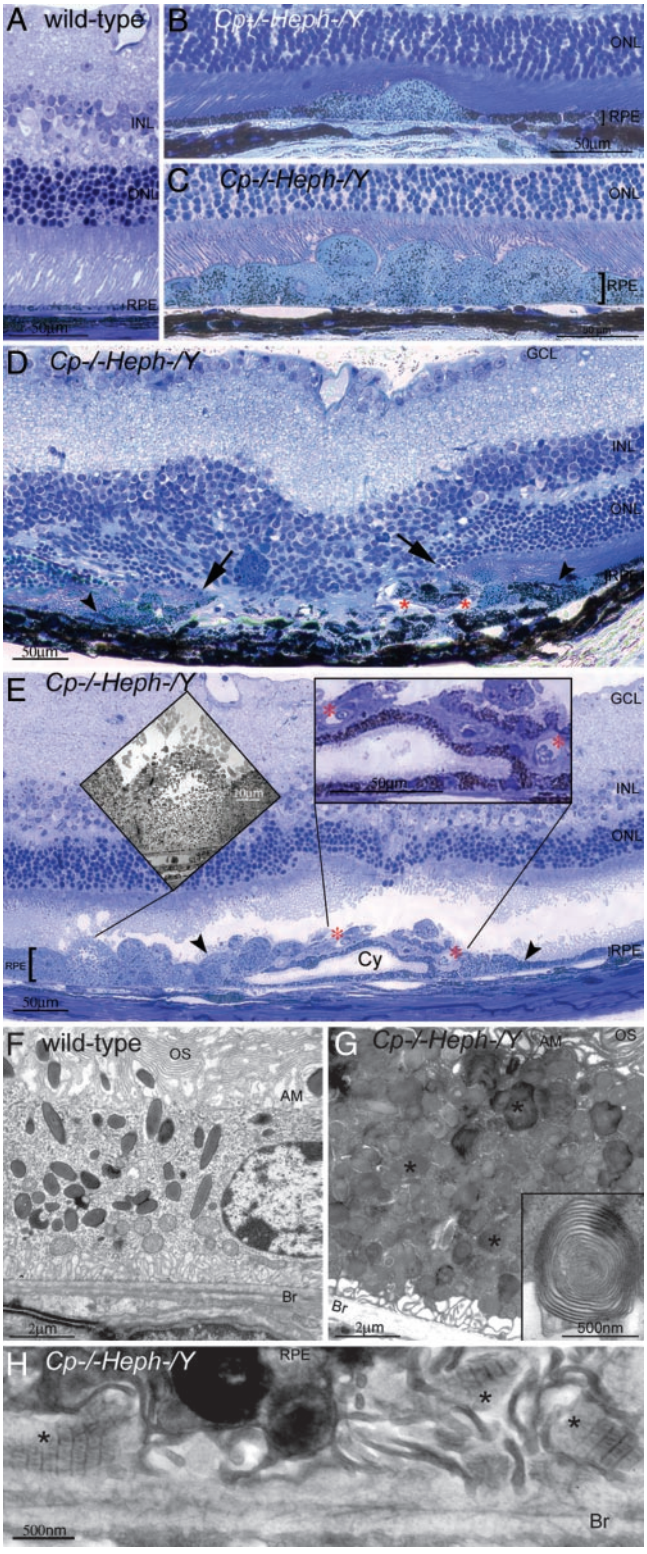

Fig. 5. Nine-month-old *Cp−/−Heph−/Y* mice have retinal degeneration. (*A*) Light photomicrograph of WT retina. (*B* and *C*) *Cp−/−Heph−/Y* retina has focal patches of hypertrophic RPE cells in some areas (*B*) and confluent hypertrophic RPE cells in other areas (*C*). (*D*) In an area of RPE hyperplasia (demarcated by arrowheads), *Cp−/−Heph−/Y* retinas have local photoreceptor degeneration [demarcated by arrows in the outer nuclear layer (ONL)] and subretinal neovascularization (red *). (*E*) In an area of hypertrophic, hyperplastic (area demarcated by arrowheads) RPE cells, a necrotic RPE cell also observed by electron microscopy (*Left Inset*) is present. Within the area of RPE hyperplasia, there is local photoreceptor thinning and subretinal neovascularization (red *) visible as small vessels containing erythrocytes (*Right Inset*). The hyperplastic RPE have formed a localized cyst (Cy). (*F*) Electron micrograph of WT RPE. Br, Bruch's membrane; AM, apical microvilli; OS, photoreceptor outer segments. (*G*) Electron micrograph of *Cp−/−Heph−/Y* RPE overloaded with phagosomes and lysosomes containing photoreceptor outer segments at various stages of digestion. Some of these lysosomes (*) contained multilamellar structures characteristic of outer segment membranes (*Inset*). (*H*) Electron micrograph of *Cp−/−Heph−/Y* deposits between RPE and Bruch's membrane containing wide-spaced collagen (*). (Scale bars: *A–E*, 50 μm; *F* and *G*, 2 μm; H, 500 nm.)

In addition to these areas of hypertrophic RPE with a normal appearing neural retina, within each eye there were also a few focal areas of extensive RPE hyperplasia and necrosis (Fig. 5 *D* and *E*) accompanied by local photoreceptor loss and subretinal neovascularization. Focal areas of subretinal deposits were also observed at the ultrastructural level. Clusters of these deposits spanned regions ranging from 50 to 500 μm and contained banded structures with a periodicity of 110 nm (Fig. 5*H*), similar to the wide-spaced collagen observed in basal laminar deposits in AMD retinas.

Discussion

Cp and Heph ferroxidases are believed to facilitate iron export from cells by oxidizing ferrous to ferric iron, the only form that can be taken up by the serum transport protein transferrin. Although *Cp* is up-regulated after stress in multiple tissues, including retina (11, 12), and although Cp is necessary for iron export from brain astrocytes *in vitro* (13), the role of *Heph* in the CNS and its functional relationship to *Cp* had not been characterized.

We demonstrate that *Cp* and *Heph* serve essential functions in retinal iron regulation. In the normal mouse, both ferroxidases are present in the RPE and retina. In the retinas of *Cp−/−Heph−/Y* mice, Perls' stain detected increased iron in outer segments of *Cp−/−Heph−/Y* photoreceptors by age 5–6 months, and atomic absorption spectrophotometry demonstrated increased retinal iron compared with non- *Cp−/−Heph−/Y* retinas. In the RPE, deficiency of both ferroxidases resulted in massive iron accumulation detectable even with the unenhanced Perls' stain and quantitatively confirmed by atomic absorption spectrophotometry. At age 6–9 months, some *Cp−/−Heph−/Y* mice developed retinal degeneration and neovascularization, emphasizing the importance of proper iron metabolism for retinal health.

Only mice with deficiency of both Cp and Heph developed retinal iron overload and degeneration. One potential mechanistic explanation for the iron overload is that Cp and Heph, which we show are both expressed in Muller glia and RPE cells, may facilitate iron export from the plasma membrane of these cells. Alternatively, they may mediate iron export from different intracellular compartments, with combined deficiency resulting in significant iron overload. Future studies with subcellular immunolocalization should shed light on this issue.

Age-Dependent Iron Overload in *Cp−/−Heph−/Y* Mice. The striking iron overload in the *Cp−/−Heph−/Y* mice occurs despite Heph deficiency-induced impairment of intestinal iron uptake, which causes low serum iron levels and anemia (17). At 5–6 months, *Cp−/−Heph−/Y* RPE contained iron-laden vesicles. Iron is normally taken into lysosomes of the RPE by endocytosis of transferrin-bound iron (24) or phagocytosis of iron-laden shed outer segments (25). These lysosomes fuse with melanosomes in RPE (26), potentially explaining the presence of fused iron-laden vesicle/melanosomes in the *Cp−/−Heph−/Y* RPE.

Elevation of iron levels in *Cp−/−Heph−/Y* retinas resulted in increased levels of the cytosolic iron storage protein ferritin. Increased L-ferritin was observed in the *Cp−/−Heph−/Y* RPE, consistent with the Perls' label, but H-ferritin was not detectable in *Cp−/−Heph−/Y* RPE. Differential expression of these ferritin

subunits is not unusual (27); liver, for example, expresses primarily L-ferritin, whereas heart expresses primarily H-ferritin (28).

Mechanistic and Structural Similarities Between *Cp−/−Heph−/Y* Retinas and Human Retinal Degeneration. Although histopathology of human retinal degeneration in aceruloplasminemia has not been described, clinical examination of an aceruloplasminemic Caucasian shows early-onset drusen, and fluorescein angiography of a Japanese aceruloplasminemic patient suggests RPE degeneration just peripheral to the macula, the central part of the retina. The histology of the 6- to 9-month-old *Cp−/−Heph−/Y* mouse retina may shed light on mechanisms of RPE degeneration and drusen formation in aceruloplasminemia. Like the murine *Cp−/−Heph−/Y* RPE, the RPE in human aceruloplasminemia is likely to be iron-overloaded, accumulate lysosomes, and eventually die. Unlike human aceruloplasminemia and *Cp−/−Heph−/Y* mice, retinas from *Cp−/−* mice do not exhibit RPE degeneration. This discrepancy could be explained by a very slow RPE iron accumulation caused by the absence of Cp in both mouse and human, too slow to cause RPE degeneration in the short lifespan of a mouse.

The subretinal neovascularization in *Cp−/−Heph−/Y* retinas has not been reported in patients with aceruloplasminemia, but does occur in other human retinal degenerations. AMD is thought to result from primary RPE death leading to secondary photoreceptor death, as appears to be the case in *Cp−/−Heph−/Y* retinas, and the progression of AMD to its wet form results in subretinal neovascularization, also seen in *Cp−/−Heph−/Y* eyes. Subretinal neovascularization in AMD most often originates from the choroid, with occasional contributions from the retinal circulation; the source of subretinal neovascularization in *Cp−/−Heph−/Y* eyes awaits further investigation. Other similarities between AMD and the *Cp−/−Heph−/Y* mouse are the presence of sub-RPE widespaced collagen (Fig. 5), a component of drusen, RPE lysosomal inclusions and death, and elevated levels of RPE iron (4). Despite the histologic similarities between the *Cp−/−Heph−/Y* mouse and AMD, the *Cp−/−Heph−/Y* mouse is not an exact phenocopy of AMD, as it lacks clinically observable drusen, and AMD retinas do not have such extensive RPE hypertrophy. Further, whereas several pieces of evidence suggest that iron overload may contribute to AMD [elevated iron levels in postmortem AMD retinas (4), early-onset drusen in an aceruloplasminemic patient (J.L.D., unpublished data), and some histologic features of AMD in *Cp−/−Heph−/Y* mice], further work is needed to test the role of iron overload in AMD. Mice with defects in macrophage recruitment develop sub-RPE deposits and choroidal neovascularization (29). It is possible that the combination of increased production of oxidized molecules, most likely a cause of retinal degeneration in the *Cp−/−Heph−/Y* mouse, and decreased clearance of such materials by macrophages can lead to AMD.

Implications for the CNS. Disordered iron metabolism has been implicated in both common and rare neurodegenerations. Elevated iron levels have been detected in Alzheimer's- and Parkinson's-affected brains and AMD-affected retinas (4, 30). The possibility that iron chelation may be therapeutic in such patients is supported by experiments in which iron chelation by either transgenic expression of the iron-binding protein ferritin or oral administration of the bioavailable metal chelator clioquinol reduced the severity of neurodegeneration in a mouse model of Parkinson's disease (31). Our *Cp−/−Heph−/Y* mice with iron overload-induced retinal degeneration provide an opportunity to test the efficacy of iron chelators and antioxidants for neuroprotection. Further, because *Cp−/−Heph−/Y* mice have limited viability as they approach 6–9 months of age, limiting the number of mice that live long enough to develop retinal degeneration, an RPE-specific conditional *Heph* knockout will facilitate investigation into the frequency and extent of pathology and other studies of age-dependent retinal degeneration. In summary, these data demonstrate that *Cp* and *Heph* are mediators of iron metabolism in a CNS site, the retina, such that deficiency of both yields a massive iron accumulation and corresponding RPE/retinal pathology.

We thank Robert Wong, Carrie Hegedus, Neelima Shah, Raymond Meade, Qian-Chun Yu, Melanie Minda, and John Tomaszewski for advice and assistance. This work was supported by a Research to Prevent Blindness (Career Development Award to J.L.D. and an unrestricted grant), the International Retina Research Foundation, National Institutes of Health/National Eye Institute Grants EY015240 and EY00417, National Institute of Diabetes and Digestive and Kidney Diseases Grants DK02464 and DK58086, the Steinbach Foundation, and the F. M. Kirby Foundation.

1. Doly, M., Bonhomme, B. & Vennat, J. C. (1986) *Ophthalmic Res.* **18,** 21–27.
2. Vergara, O., Ogden, T. & Ryan, S. (1989) *Exp. Eye Res.* **49,** 1115–1126.
3. Tawara, A. (1986) *Invest. Ophthalmol. Visual Sci.* **27,** 226–236.
4. Hahn, P., Milam, A. H. & Dunaief, J. L. (2003) *Arch. Ophthalmol.* **121,** 1099–1105.
5. Miyajima, H., Nishimura, Y., Mizoguchi, K., Sakamoto, M., Shimizu, T. & Honda, N. (1987) *Neurology* **37,** 761–767.
6. Morita, H., Ikeda, S., Yamamoto, K., Morita, S., Yoshida, K., Nomoto, S., Kato, M. & Yanagisawa, N. (1995) *Ann. Neurol.* **37,** 646–656.
7. Yamaguchi, K., Takahashi, S., Kawanami, T., Kato, T. & Sasaki, H. (1998) *Ophthalmologica* **212,** 11–14.
8. Patel, B. N. & David, S. (1997) *J. Biol. Chem.* **272,** 20185–20190.
9. Klomp, L. W. & Gitlin, J. D. (1996) *Hum. Mol. Genet.* **5,** 1989–1996.
10. Klomp, L. W., Farhangrazi, Z. S., Dugan, L. L. & Gitlin, J. D. (1996) *J. Clin. Invest.* **98,** 207–215.
11. Levin, L. A. & Geszvain, K. M. (1998) *Invest. Ophthalmol. Visual Sci.* **39,** 157–163.
12. Chen, L., Dentchev, T., Wong, R., Hahn, P., Wen, R., Bennett, J. & Dunaief, J. L. (2003) *Mol. Vis.* **9,** 151–158.
13. Jeong, S. Y. & David, S. (2003) *J. Biol. Chem.* **278,** 27144–27148.
14. Sarkar, J., Seshadri, V., Tripoulas, N. A., Ketterer, M. E. & Fox, P. L. (2003) *J. Biol. Chem.* **278,** 44018–44024.
15. Harris, Z. L., Durley, A. P., Man, T. K. & Gitlin, J. D. (1999) *Proc. Natl. Acad. Sci. USA* **96,** 10812–10817.
16. Patel, B. N., Dunn, R. J., Jeong, S. Y., Zhu, Q., Julien, J. P. & David, S. (2002) *J. Neurosci.* **22,** 6578–6586.
17. Vulpe, C. D., Kuo, Y. M., Murphy, T. L., Cowley, L., Askwith, C., Libina, N., Gitschier, J. & Anderson, G. J. (1999) *Nat. Genet.* **21,** 195–199.
18. Chen, H., Attieh, Z. K., Su, T., Syed, B. A., Gao, H., Alaeddine, R. M., Fox, T. C., Usta, J., Naylor, C. E., Evans, R. W., *et al.* (2004) *Blood*, in press.
19. Dunn, K. C., Aotaki-Keen, A. E., Putkey, F. R. & Hjelmeland, L. M. (1996) *Exp. Eye Res.* **62,** 155–169.
20. Erikson, K. M., Pinero, D. J., Connor, J. R. & Beard, J. L. (1997) *J. Nutr.* **127,** 2030–2038.
21. Rawson, A. J., Patton, G. W., Hofmann, S., Pietra, G. G. & Johns, L. (1993) *Ecotoxicol. Environ. Saf.* **25,** 41–47.
22. Dunaief, J. L., Dentchev, T., Ying, G. S. & Milam, A. H. (2002) *Arch. Ophthalmol.* **120,** 1435–1442.
23. Rouault, T. & Klausner, R. (1997) *Curr. Top. Cell. Regul.* **35,** 1–19.
24. Hunt, R. C. & Davis, A. A. (1992) *J. Cell. Physiol.* **152,** 102–110.
25. Yefimova, M. G., Jeanny, J. C., Keller, N., Sergeant, C., Guillonneau, X., Beaumont, C. & Courtois, Y. (2002) *Invest. Ophthalmol. Visual Sci.* **43,** 537–545.
26. Schraermeyer, U., Peters, S., Thumann, G., Kociok, N. & Heimann, K. (1999) *Exp. Eye Res.* **68,** 237–245.
27. Han, J., Day, J. R., Connor, J. R. & Beard, J. L. (2002) *J. Nutr.* **132,** 2769–2774.
28. Aisen, P., Enns, C. & Wessling-Resnick, M. (2001) *Int. J. Biochem. Cell Biol.* **33,** 940–959.
29. Ambati, J., Anand, A., Fernandez, S., Sakurai, E., Lynn, B. C., Kuziel, W. A., Rollins, B. J. & Ambati, B. K. (2003) *Nat. Med.* **9,** 1390–1397.
30. Perry, G., Sayre, L. M., Atwood, C. S., Castellani, R. J., Cash, A. D., Rottkamp, C. A. & Smith, M. A. (2002) *CNS Drugs* **16,** 339–352.
31. Kaur, D., Yantiri, F., Rajagopalan, S., Kumar, J., Mo, J. Q., Boonplueang, R., Viswanath, V., Jacobs, R., Yang, L., Beal, M. F., *et al.* (2003) *Neuron* **37,** 899–909.